Biosensors and Bioelectronics 141 (2019) 111474

Contents lists available at ScienceDirect

Biosensors and Bioelectronics

journal homepage: www.elsevier.com/locate/bios

A new electrochemical sensor for simultaneous determination of arbutin and vitamin C based on hydroxyapatite-ZnO-Pd nanoparticles modified carbon paste electrode

Seyed Alireza Shahamirifard, Mehrorang Ghaedi*

Department of Chemistry, Yasouj University, Yasouj, 75918-74831, Iran

ARTICLE INFO

Keywords:
Arbutin
Vitamin C
Modified carbon paste electrode
Hydroxyapatite

ABSTRACT

A highly sensitive and selective sensor was fabricated based on Hydroxyapatite-ZnO-Pd NPs modified carbon paste electrode (HAP- ZnO–Pd NPs/CPE) for simultaneous determination of Arbutin (AT) and vitamin C (VC) for the first time. Characterization was performed by Fourier transform infrared spectroscopy, X-ray diffraction, field emission scanning electron microscopy and energy dispersive X-ray spectroscopy. The modified electrode was studied by different methods including electrochemical impedance spectroscopy and cyclic voltammetry. The HAP- ZnO–Pd NPs/CPE exhibited excellent electrocatalytic activity towards the oxidations of AT and VC in phosphate buffer solution (pH 7.0) and the corresponding electrochemical signals have appeared as two well resolved oxidation peaks with significant peak potential differences of 0.23 V. Kinetic parameters such as charge transfer coefficient (0.52 and 0.44 for AT and VC respectively), standard heterogeneous electron transfer rate constant (0.336 s^{-1} and 0.590 s^{-1} for AT and VC respectively), and other electrochemical parameters were calculated via voltammetry techniques. Differential pulse voltammetry was used for simultaneous determination of AT and VC using the HAP- ZnO–Pd NPs/CPE electrode. At the optimum conditions, for simultaneous determination by synchronous change of the analyte concentrations, the linear response ranges were between 0.12–56 μM for AT and 0.12–55.36 μM for VC with detection limits of 85.7 and 19.4 nM respectively while sensitivity of proposed sensor for AT and VC was 0.98 μA/μM and 0.94 μA/μM. Reproducibility (intra-; 1.16% and 1.16% for AT and VC respectively and inter-electrode reproducibility of 2.03% and 3.28 for AT and VC respectively), and response time about 3.5 min were obtained. Furthermore, HAP- ZnO–Pd NPs/CPE was successfully applied for the independent determination of VC in fruit juice as well as the simultaneous determination of AT and VC in lightening cream samples.

1. Introduction

Arbutin (AT), or hydroquinone-b-D-glucopyranoside is derived of plants such as thyme, bearberry, marjoram, pear, cranberry also several kinds of cereals (Clifford, 2000) that is used in beauty industry as skin whitening, depigmenting cosmetics and anti-sunburn of human skin (Gallarate et al., 2004). The AT by inhibiting melanogenesis in melanoma cells can play useful role and remove melanin disorders. Tyrosinase is the required enzyme for melanin formation and accumulation of melanin in subcutaneous tissue produced via a tyrosinase-catalyzed metabolic pathway and AT reduce cellular tyrosinase activity without changing the cell viability that is followed the depigmenting effect of arbutin (Maeda and Fukuda, 1991). The cosmetic effect of AT, as glycosidic form of hydroquinone, is weaker than hydroquinone but hydroquinone shows cytotoxicity, nephrotoxicity, and genotoxicity while toxicity of AT is strongly diminished, therefore AT widely used as active agent in the whitening cosmetic creams (Maeda and Fukuda, 1991). Moreover, some bacteria and other microorganisms in human skin such as Staphylococcus epidermidis and *Staphylococcus aureus* can change bioactivity of AT through hydrolyze it (Akiyama et al., 2000; Bang et al., 2008; Keyworth et al., 1992; Kozitskaya et al., 2005; O'gara and Humphreys, 2001). Vitamin C (VC) or known Ascorbic acid is a water-soluble vitamin which exists extensively in fruits, vegetables, animal feed, pharmaceutical formulations, multivitamin tablets and especially in cosmetic applications as an antioxidant. VC plays an important role in biological metabolisms, which is conducive to free radical and blocked it therefore prevent of damages such as damage DNA and it caused cell development. The VC also plays a key role in therapeutic field such as healing injuries or burns, preventing cancer and improving immunity while low levels of VC can result in a condition called scurvy.

* Corresponding author.
E-mail addresses: mahtamatin@gmail.com (S.A. Shahamirifard), m_ghaedi@mail.yu.ac.ir (M. Ghaedi).

https://doi.org/10.1016/j.bios.2019.111474
Received 19 March 2019; Received in revised form 14 June 2019; Accepted 23 June 2019
Available online 28 June 2019

Scurvy may cause symptoms such as muscle rash, tiredness, tooth loss, joint pain or weakness (Jiang and Du, 2014). In some cosmetic creams such as Seagull Herbal Lightening Cram for development properties of them there is both AT and VC in addition to other vitamins. Determination of AT have been carried out via methods such as HPLC-UV(Wang et al., 2015), HPLC with photodiode array detection (Jeon et al., 2015) capillary electrophoresis with a glassy carbon electrode (Blasco et al., 2005) and electrochemical methods (Libánský et al., 2011; Shih and Zen, 2000). Various methods for detection and determination of VC have been developed such as HPLC (Klimczak and Gliszczyńska-Świgło, 2015), spectroscopy (Fong et al., 2016), Amperometry (Su et al., 2017) and voltammetry (Arabali et al., 2016) while chromatography and spectrophotometry have some major problems in analytical analysis such as complexity and the time consuming nature of the analysis process. Therefore, researchers focused on electrochemical methods (Najafi et al., 2014). Among working electrodes in electrochemical systems, carbon paste electrode (CPE) is widely used because of having several advantages such as easy modification, regenerable surface, low background current, extreme potential window, low ohmic resistance and low cost (Jahani and Beitollahi, 2016). The improvement of electrodes performance has been carried out by their modification, by hydroxyapatite (HAP) due to specifically properties such as its excellent biocompatibility, slow biodegradation, good mechanical stability, great absorption property non-toxic, non-inflammatory and non-immunogenic material which makes it a very attractive material for bioelectrochemical sensor systems (Yang and Zhang, 2011) and also nanomaterials such as metal and metal oxide nanoparticles due to high surface-to-volume ratio, good conductivity and electrocatalysis features (Liu et al., 2017). For example, palladium and zinc oxide nanoparticles show unique properties for several applications in different fields of electrochemistry by providing an improvement in mass transport and enhancing catalytic processes (Liu et al., 2017; Rahmanpour and Khalilzadeh, 2016). A layer of HAP may provide good surface for immobilization of nano structure material on electrode surface due to easy to functionalize. (Zhao et al., 2009) and also it make conditions for facilitating electron-transfer process via synergistic action between itself and mediator. Furthermore, HAP supported palladium complexes have been reported as efficient heterogeneous catalyst for the oxidation of alcohol (Mori et al., 2002) But there have been no reporte about HAP applied in the fabrication of voltammetry sensor to simultaneous determination of AT and VC. Herein, we report, for the first time, the construction of new electrochemical sensor using nano composite contain HAP, PdNPs and ZnONPs to fabricate modified carbon paste electrode for simultaneous determination of AT and VC. The proposed method exhibits many advantages such as fast response, low detection limit, large dynamic range and good selectivity. Utilizing the developed method, the determination of AT and VC is carried out in fruit juice and cosmetic cream samples.

2. Experimental

2.1. Apparatus and materials

The electrochemical measurements were performed using an Autolab potentiostat/galvanostat (PGSTAT-302N, Eco Chemie, Netherlands). All experiments were performed using a three-electrode system including Ag/AgCl/KCl (3.0 M) electrode, a platinum wire (Metrohm, Netherlands) and the HAP-ZnO-PdNPs/CPE as reference, auxiliary and working electrodes, respectively. All potentials are quoted versus Ag/AgCl (3.0 M KCl) reference electrode. pH/Ion meter model 686 (Metrohm, Switzerland, Swiss) was used for pH adjustment. For characterization, Fourier transform infrared spectroscopy (FT-IR JASCO 460 Plus, Mexico), X-ray diffraction (XRD) (Philips, 40 mA and 40 kV, Anode Material: Cu, Netherland) and field emission scanning electron microscopy (FE-SEM: Sigma, Zeiss, Germany) were used. AT, VC and other reagents of analytical grade were purchased from Merck (Darmstadt, Germany). Graphite powder and paraffin oil (DC 350, density = 0.88 g cm^{-3}) as binding agent (Merck, Darmstadt, Germany) were used for preparing the pastes.

2.2. Preparation of HAP, HAP-ZnO NPs and HAP-ZnO-Pd NPs

In a typical synthesis, HAP powder was synthesized according to pervious reports: phosphoric acid solution (0.5M) was slowly added into saturated solution of Calcium hydroxide ($Ca(OH)_2$) and then pH adjusted to 8.2 by sodium hydroxide solution (2M) while the mixture of reaction was vigorously stirred for 12 h (suspension 1). Calcination carried out for 2 h at 400 °C in oven after filtration of solution and drying it. For preparation of HAP-ZnO NPs, zinc nitrate solution (0.267 g ml^{-1}), as the source of Zn^{2+} ions, were added to suspension 1 and then was repeated next steps similar to pervious synthesis. HAP-ZnO-Pd NPs was prepared by adding zinc nitrate solution (0.267 g ml^{-1}) and palladium nitrate (0.027 g ml^{-1}) to suspension 1 while pH of mixture was adjusted to 8 by sodium carbonate solution and then was repeated next steps similar to preparation of HAP (Kanchana et al., 2014; Yao et al., 2014).

2.3. Synthesis of Pd/ZnO nanoparticles

For preparation of Pd/ZnO nanoparticles via co-precipitation method, an aqueous solution of sodium carbonate (1 M) was added to a mixture of zinc nitrate (0.267 g mL^{-1}) and palladium nitrate (0.027 g mL^{-1}) solutions, at room temperature until pH of solution was adjusted to 8. The precipitates were filtered, washed several times with distilled water and absolute ethanol after 2 h aging at 70–80 °C and dried at 80 °C and then calcinated at 723 K for 2 h (Hosseini-Sarvari and Razmi, 2015).

2.4. Preparation of modified carbon paste electrode

The HAP-ZnO-Pd NPs carbon paste electrode was prepared by mixing 75% (w/w) of HAP-ZnO-Pd NPs and graphite powder (HAP-ZnO-Pd NPs:graphite powder 10:90%) with 25% (w/w) of paraffin in a mortar and pestle. 0.10 g of the mixture was homogenized in a mortar for 30 min and the resulted composite was dispersed in tetrahydrofuran (THF) followed by magnetic stirring until the complete evaporation of solvent and drying for 24 h. Finally, the homogenized paste was then inserted into a hole of Teflon tube of diameter 3.0 mm and depth 2.0 mm. Electrical connection was implemented by a copper wire of diameter 1.0 mm fitted into the tube. A fresh electrode surface was obtained by squeezing out a small portion of the paste and polishing it by filter paper until a smooth surface was obtained.

3. Results and discussion

3.1. Characterization of HAP-ZnO-Pd NPs

According to FT-IR spectrum of HAP (Fig. S1a), a band around 3440 cm^{-1} (peak 1) assigned to the elongation vibrations of $OH-$ groups located in the tunnels of the apatite due to adsorption of moisture on its surface, the bands located in the 1300–1600 cm^{-1}region (peaks of 2–4) and those with weak intensity appearing at 1415 $cm^{-1}$and 1455 $cm^{-1}$are attributed to the carbonates resulting from the atmospheric CO_2 adsorbed by the apatite. The $(PO_4)^{3-}$species are characterized by a band appearing at 1037 cm^{-1} (peak 5), the bands in the 566–601 cm^{-1} (peaks of 6 and 7) domain are ascribed to the deformation vibrations of O–P – O groups (Takarroumt et al., 2013). The X-ray diffraction patterns of the synthesized HAP (Fig. S1b) shows that the solids are monophasic and good agreement with the crystallographic planes of hexagonal belonging to the $P6_3/m$ space group (ICSD, no. 09–0432). XRD pattern of HAP-ZnO NPs was compared with HAP-ZnO-Pd NPs (Fig. S2a and Fig. S2b) and have not

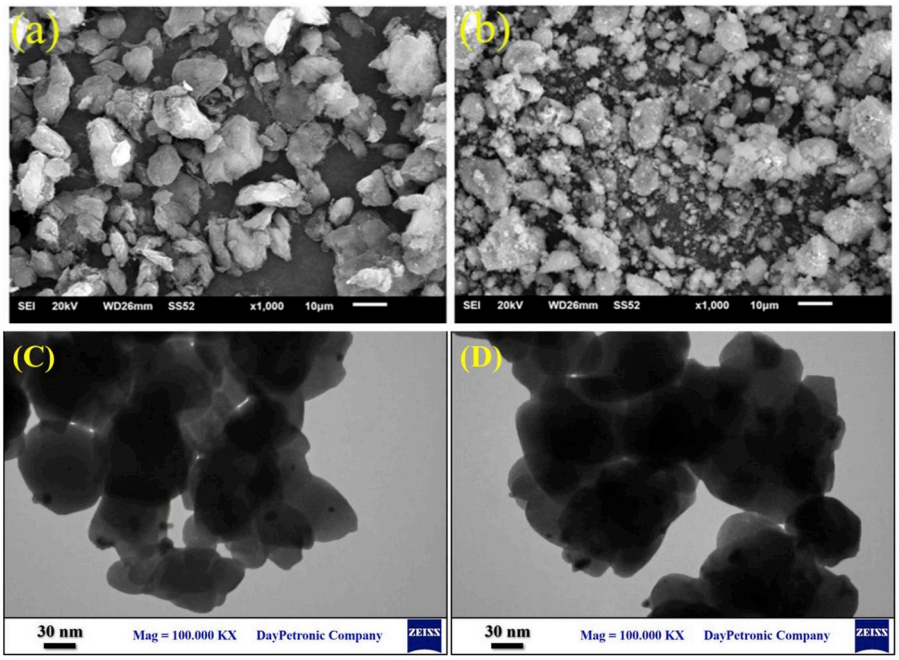

Fig. 1. (a) and (b) FE-SEM images of uncoated HAP and HAP-ZnO-Pd NPs respectively, (C) and (D) TEM image of uncoated HAP and HAP-ZnO-Pd NPs respectively.

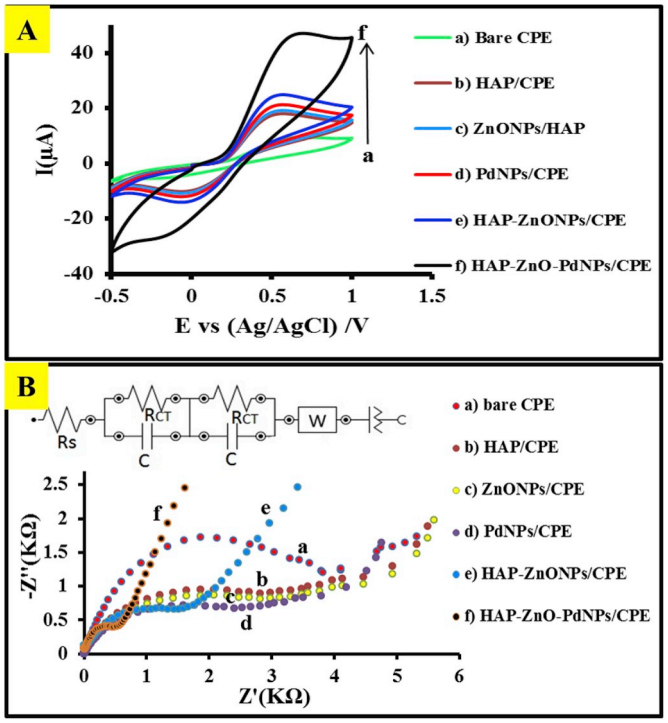

Fig. 2. (A) CVs and **(B)** Nyquist plots of different electrodes: (a) bare, (b) HAP/CPE, (c) ZnO NPs/CPE (d) Pd NPs/CPE (e) HAP-ZnO NPs/CPE and (f) HAP-ZnO-Pd NPs/CPE in a 0.1 M KCl solution containing 5 mM M $Fe(CN)_6^{3-/4-}$. Inset **(B)**: modified Randles equivalent circuit.

approximately been observed significant difference due to probably excellent stability hexagonal HAP and the other hand amount of loaded nanoparticles on HAP surface were few. Fig. 1 (a and b) shows FE-SEM images of HAP and modified HAP by Pd–ZnO NPs respectively. Fig. 1a shows size of HAP is in order to micrometer and its shape is hexagonal but a significant difference in the surface morphology has been observed between Fig. 1a and b that it demonstrates successful loading ZnO–Pd NPs on surface of HAP. And also TEM image of HAP and HAP-ZnO-PdNPs was investigated that images were shown in Fig. 1(C and D). As can be seen in TEM images, obtained results are in agreement with XRD analysis results which crystallographic planes are hexagonal. The elemental analysis of HAP and HAP-Pd-ZnONPs were confirmed by energy dispersive X-ray analysis (EDX) and X-ray fluorescence spectroscopy (XRF) technique. EDX quantitative analysis was performed in the marked area in the secondary electron image. The result of EDX microanalysis of the HAP and HAP-Pd-ZnONPs are shown in Fig. S3. The peaks of O, P and Ca indicate the consisting elements of synthesized HAP and EDX spectrum of HAP-Pd-ZnONPs sample is contain the peaks of O, P, Ca, Zn and Pd which it confirms successfully loading Pd-ZnONPs on HAP surface. X-ray fluorescence (XRF) spectroscopy is analytical technology widely used in geology for metallic elements detection in complicated samples due to its high sensitivity, specificity and simplicity therefore the existent elements in prepared HAP and HAP-Pd-ZnONPs and estimated composition were measured by XRF as nondestructive method. The results clearly indicated to existence of O, P, Ca, in HAP and O, P, Ca, Zn and Pd in synthesized HAP-Pd-ZnONPs samples (Table S1). According to Table S2 and comparison of amount element (W/W%) in two samples, It was observed that the P, Ca percentage decreased in HAP-Pd-ZnONPs versus HAP which it prove loading of Pd-ZnONPs on HAP surface. Chemical characterization of modified carbon paste by HAP-ZnO-Pd NPs was investigated by Energy-dispersive X-ray spectroscopy (EDX) technique and it confirmed presenting of C, Ca, P, Zn, Pd and O elements in it (Fig. S3).

3.2. Electrochemical behavior of HAP-ZnO-Pd NPs/CPE electrode

To investigate the performance of the HAP-ZnO-Pd NPs/CPE, several modified electrodes including bare, HAP/CPE, HAP-ZnONPs/CPE and HAP-ZnO-PdNPs/CPE were studied by cyclic voltammetry (CV) and electrochemical impedance spectroscopy (EIS) in a 0.1 M KCl solution containing of a redox probe (5 mM $K_4Fe(CN)_6$ and 5 mM $K_3Fe(CN)_6$ solution). As shown in Fig. 2A, HAP-ZnO-PdNPs/CPE (curve d) resulted in the peak current (Ipa) of 3.54, 2.81 and 1.97 times of that of the bare

electrode (curve a), HAP/CPE (curve b) and HAP-ZnONPs/CPE (curve c), respectively. The enhancement in Ipa of HAP/CPE compared with bare electrode may be due to the high electron transfer kinetics, high surface area and good conductivity of HAP/CPE, which accelerate electron transfer processes between $Fe(CN)_6^{3-/4-}$ and CPE. The increase in Ipa of the HAP-ZnONPs/CPE is due to the effective present of ZnONPs in electrode and development of conductivity and effective surface area of electrode (curve c) and more attraction of $Fe(CN)_6^{3-/4-}$ on surface electrode. According to pervious reports, ZnO nanoparticle was also implemented to adsorb components such as arbutin and vit C that have carboxylic or hydroxyl groups by bridging, ester-like or bidentate and the formation of AT/ZnO or VC/ZnO exhibited a slight increase in the excited-state oxidation potential for AT and VC in comparison with the AT and VC solution (Rochford et al., 2007). Curve d shows an strong improvement in Ipa of HAP-ZnO-Pd NPs/CPE and decrease in peak separation (ΔEp) compared with that obtained for other electrodes, which demonstrate effective increase in electron transfer rate constant of $Fe(CN)_6^{3-/4-}$ redox reaction due to the presence of PdNPs on the HAP-ZnO-Pd NPs/CPE. On the other hand, According to pervious reports, ZnO was used as carrier for Pd nanoparticles to form Pd–ZnO nanostructures, which showed strikingly different catalytic activities compared to the bare ZnO NPs (Arroyo-Ramírez et al., 2014).

The investigation of interfacial characteristics of the differently modified electrodes was studied by EIS. The interfacial behavior is widely descripted by modified Randles equivalent circuit (inset of Fig. 2B). In such model, the constant phase element (CPE) is in series with Warburg impedance (w) and solution resistance (Rs). In the purposed equivalent circuit are two charge transfer resistance (Rct) and two capacitances (C) in parallel. Modified Randles model was used to fit the EIS data. The impedance spectra as Nyquist plots for CPE (a), HAP/CPE (b), HAP-ZnONPs/CPE (c) and HAP-ZnO-Pd NPs/CPE (d) are shown in Fig. 2B.The Rct depends on the electron transfer kinetics of the redox probe at the surface of the purposed electrode that is obtained from the diameter of semicircle in the Nyquist plot. According Fig. 2B, Rct of (a) to (d) curves was obtained to be 4.26, 2.82, 2.12 and 0.45 KΩ, respectively. Liquid paraffin in the bare CPE increases electron transfer resistance to 4.26 KΩ because it is non-conductive. The value of Rct reduces from (b) to (d) because of the increase in effective surface area, conductivity and electron transfer rate constant. Thus, this modified electrode was selected as optimized electrode for more electrochemical studies.

3.3. Electrocatalytic properties of the HAP-ZnO-Pd NPs/CPE

The quality of the modified electrode for oxidation of AT and VC was investigated by cyclic voltammetry in a solution containing AT (55 μM) and phophate buffer solution (PBS) at pH 7. CVs were recorded in the potential range of −0.2–1.2 V. Fig. 3A shows the comparison of electrocatalytic oxidation towards AT at the stepwise modified electrodes. Voltammograms (a), (b), (c) and (d) correspond to bare electrode, HAP/CPE, HAP-ZnONPs/CPE and HAP-ZnO-Pd NPs/CPE, respectively. According Fig. 3A the anodic peak potential for AT oxidation at the unmodified electrode was not observed due to the stability of AT over the studied potential range. At other electodes, they were clearly observed at 0.48 V (versus Ag/AgCl electrode), respectively, indicating the presence of HAP, ZnONPs and PdNPs in the CPE. An irreversible oxidation peak current corresponding to AT, which is attributed to a one-electron oxidation process, is obviously seen in HAP/CPE due to the catalytic effect of HAP. Activated surface and conductivity of electrode increase in presence of HAP at CPE surface. Increase in anodic peak current of (c) to (d) is due to making more facility in electron transfer process and adsorption of AT on electrode surface. Also oxidation of VC at modified electrode HAP-ZnO-Pd NPs/CPE was studied via CV technique in the same condition of AT but in the potential range of −0.1–1.5 V. Fig. 3B shows the comparison of electrocatalytic oxidation of VC at the modified electrodes similar to AT. Voltammograms (a), (b), (c) and (d) correspond to bare electrode, HAP/CPE, HAP-ZnO NPs/CPE and HAP-ZnO-Pd NPs/CPE, respectively. According Fig. 3B the anodic peak potential for VC oxidation at the bare electrode was not observed due to the stability of VC over the studied potential range. At other electodes, they were clearly observed at 0.71 V (versus Ag/AgCl electrode), respectively, indicating the presence of HAP, ZnO NPs and Pd NPs in the CPE. An irreversible oxidation peak current corresponding to VC, which is attributed to a two-electron oxidation process, is patently seen in HAP/CPE due to the catalytic effect of HAP. Activated surface and conductivity of electrode increase in presence of HAP at CPE surface and also increasing anodic peak current of (c) to (d) is due to making more facility in electron transfer process and adsorption of VC on electrode surface in presence of ZnO NPs and Pd NPs in carbon paste.

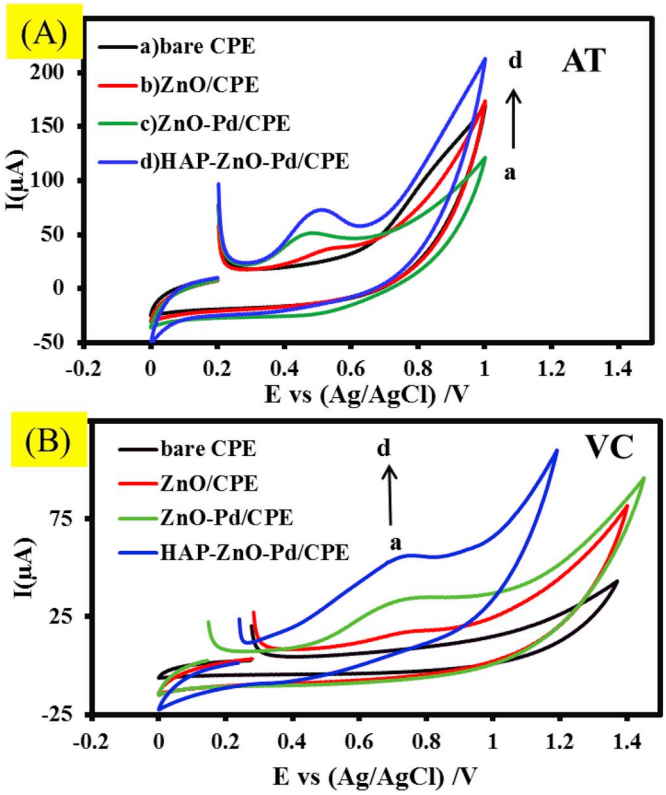

Fig. 3. CVs of (a) bare CPE, (b) HAP/CPE, (c) HAP-ZnONPs/CPE and (d) HAP-ZnO-Pd NPs/CPE electrode in 0.1 M BRB solution (pH 3.0), 0.1M KCl, GA (28 μM) and UA (40 μM) at scan rate of 0.1 Vs^{-1}.

3.4. Effect of the potential scan rate (υ)

The effect of the potential scan rate (υ) on electrochemical properties of the HAP-ZnO-Pd NPs/CPE in the range of 10–400 mV s^{-1} was studied by CV technique in probe solution (5 mM $Fe(CN)_6^{3-/4-}$) (Fig. S4). Based on the slope of I_p-$\nu^{1/2}$ plot (Ip(A) = 129.98$\upsilon^{1/2}$ + 3.2, R^2 = 0.9909) and Randles–Sevcik equation ($Ip = 2.69 \times 10^5 n^{3/2} A_{eff} D^{1/2} \nu^{1/2} C$), the effective area of HAP-ZnO-Pd NPs/CPE was estimated to be 1.26 mm^2, which was higher than other electrodes (i. e. bare electrode, HAP/CPE, HAP-ZnO NPs/CPE). In Randles–Sevcik equation, Ip is the peak current (A), n is the number of electrons transferred, A_{eff} is the effective area (cm^2), D is the diffusion coefficient of 5.0 mM $K_3Fe(CN)_6$ and 0.1 M KCl ($cm^2 s^{-1}$), ν is the scan rate ($V.s^{-1}$)

and C corresponds to the bulk concentration of the redox probe (mol cm^{-3}).

To obtain catalytic mechanism, the influence of the potential scan rate on electrocatalytic oxidation of AT and VC was studied by CV in PBS (pH = 7) at potential ranges −0.2–1.2 for AT and −0.1–1.5V for VC. According to Fig. S5, with increasing scan rate from 0.01 to 0.4 V s^{-1}, the oxidation peak potential shifts to more positive potentials that is showing irreversibility and the kinetic limitation in the electrochemical reaction of both AT and VC.

A linear relationship between I_p and $\upsilon^{1/2}$ is observed for both AT (Ip (AT) = 277.4 $\upsilon^{1/2}$ - 23.65 with R^2 = 0.9911) and VC (Ip (VC) = 195.13 $\upsilon^{1/2}$ + 12.01 with R^2 = 0.9909), which demonstrates that the electrode process is controlled by the diffusion step in the scan rate range from 0.01 to 0.10 V s^{-1} (Pakapongpan et al., 2014; Sheng et al., 2012) The diffusion coefficients of AT ($D_{AT} = 1.56 \times 10^{-7}$ cm^2s^{-1}) and VC ($D_{VC} = 2.47 \times 10^{-7}$ cm^2s^{-1}) were estimated at HAP-ZnO-Pd NPs/CPE by CV from the following equation for irreversible reaction: $I_p = 2.99 \times 10^5 n\ (\alpha n)^{1/2} A_{eff} D^{1/2} \nu^{1/2} C$, where α and C are charge transfer coefficient and bulk concentration of AT (55 μM) and VC (55 μM), respectively. Charge transfer coefficients of 0.52 and 0.44 were obtained for AT and VC, respectively, by considering that the slope of E_p–logυ plot is equal to 2.303RT/αnF. Here, n is considered to be 1e for oxidation reaction of AT and 2e for VC based on previous reports (Pakapongpan et al., 2014; Sheng et al., 2012), (Scheme S1). In E_p–logυ plot line equation for AT Epa (V) = 0.1148logυ + 0.6258 with (R^2 = 0.9904) and VC Epa (V) = 0.0664logυ + 0.7416 with R^2 = 0.9917 were obtained.

Based on the theory of Laviron, for an irreversible anodic reaction, the linear relationship between Ep and lnυ is given by the following equation:

$$Ep = E^\circ - \frac{RT}{n\alpha F}\ln\frac{RTKs}{n\alpha F} + \frac{RT}{n\alpha F}\ln\upsilon$$

where E^0 is the formal potential (V) and intercept of E–υ plot, K_s is the standard heterogeneous electron transfer rate constant and other parameters have their usual meanings. K_s values of 0.336 and 0.590 s^{-1} were obtained for AT and VC, respectively.

The surface concentration (r) of the AT and VC were calculated from the slope of I–υ or I − $\upsilon^{1/2}$ (< 0.1 V s^{-1}) and the following equation (Bard and Faulkner, 2001) $I_p = n^2F^2rA\upsilon/4RT$. The r values of AT and VC were calculated to be 2.34×10^{-8} and 4.12×10^{-9} mol cm^{-2}, respectively. These proximity of calculated values confirm that the AT and VC have similar control on the modified electrode surface.

3.5. Optimization of experimental conditions

3.5.1. Influence of pH

The electrochemical behavior of AT and VC at HAP-ZnO-Pd NPs/CPE depends on various factors such as type of supporting electrolyte and pH value. To select the best supporting electrolyte, oxidation behavior of AT and VC was investigated in acetate buffer solution (ABS) (a), phosphate buffer solution (PBS) (b), and Britton-Robinson buffer (BRB) solution (c) using DPV technique. The results show that the PBS is the best due to good separation of peak current and its anodic current (Fig. 4a). Therefore, the PBS was selected as the supporting electrolyte in this electroanalytical study.

The effect of buffer pH on the current response of HAP-ZnO-Pd NPs/CPE for the determination of AT and VC was investigated by DPV in the pH range of 2–9. As seen in Fig. 4b, the anodic peak potentials of AT and VC show a negative shift when the pH increases, indicating the involvement of protons in the electrode reactions. The linear relationship between peak potentials and pH can be expressed as: E_{pa} = 0.7683–0.048 pH with R^2 = 0.9927 for AT and E_{pa} = 1.084–0.058 pH with R^2 = 0.9936 for VC (Fig. 4c) therefore slops close to theoretical value (Nernstian value of 0.059 V). These results demonstrate equal number of protons and electrons involved in the electrode reaction (Pakapongpan et al., 2014; Sheng et al., 2012) (Scheme S1), As shown in Fig. 4d, the anodic current of AT and VC slightly increases with the increase in pH over the range 2–7, and then it decreases at higher pH to 9. A larger anodic response is obtained at about pH 7. Therefore, it was selected for further electrochemical studies.

3.5.2. Simultaneous determination of AT and VC

The main goal of this study was to develop a method with suitable separation in the simultaneous determination of AT and VC using HAP-ZnO-Pd NPs/CPE. Under the optimized conditions, simultaneous determination of AT and VC was investigated using DPV technique (Fig. 5). According to Fig. 5a, the DPV results show the variations in the concentration of AT from 0.1 μM to 56 μM and of VC from 0.12 μM to 55 μM with two well-separated anodic peaks at potentials of 0.48 and 0.71 V, corresponding to the oxidation of AT and VC, respectively. Potential difference between the two anodic peak potentials of AT and VC is 0.23 V that is high enough for the simultaneous determination of the concentration of AT and VC. The linear relationship between Ip(ÎM) and analyts can be expressed as follows: I_{pa}(AT) = 0.9878 [AT] (μM) + 5.1548 with R^2 of 0.9908 and I_{pa}(VC) = 0.9382 [VC] (μM) + 4.7718 with R^2 of 0.9917. The linear ranges for the determination of AT (0.12–56 μM) and VC (0.12–55.36 μM) were determined with detection limits of 85.7 and 19.4 nM, respectively, at S/N = 3. According to slope of calibration curve the sensitivity of proposed sensor for AT and VC was 0.98 μA/μM and 0.94 μA/μM. Independency on the oxidation processes of AT and VC and determination of them in binary mixture was investigated and for this purpose, VC concentration was varied over 28–38 μM in the presence of fixed concentration of AT (28 μM) (Fig. 5b) through which the VC was determined. Moreover, for the determination of AT, its concentration was varied over 15–45 μM in the presence of constant concentration of VC (38 μM) (Fig. 5c). Therefore, As seen, the simultaneous determination of AT and VC is possible without any significant interference. The analytical parameters that come from the quantitative calibration curves were summarized in Table S2.

3.6. Repeatability, reproducibility and stability study

The repeatability, reproducibility and stability of the prepared electrochemical sensor were studied through DPV under optimized conditions. The HAP-ZnO-Pd NPs/CPE was used six times sequentially for measuring 28 μM of AT and VC solution where no obvious change in DPV response was observed. The relative standard deviations (RSD) of AT and VC were obtained to be 1.96 and 0.69%, respectively, indicating desirable repeatability of the purposed sensor. The ability to create a reproducible electrode was additionally evaluated by DPV. For investigation of reproducibility, 6 successive determinations were considered and RSD% values estimated. The RSD% of intra-electrode was about 1.16 and 1.71 for AT and VC respectively and also inter-electrode RSD% was about 2.03% for AT and 3.28% for VC. The stability of the designed electrochemical sensor was also investigated. The electrodes were stored for three weeks in atmosphere, and no considerable fluctuation in peak current was observed (4.8% and 4.6% for AT and VC, respectively), indicating the good stability of the HAP-ZnO-Pd NPs/CPE electrode in optimized conditions. The response time of proposed sensor was investigated in optimum conditions and it was obtain of 3.5 min.

3.7. Interference study

Possible interferences for the detection of AT and VC at HAP-ZnO-

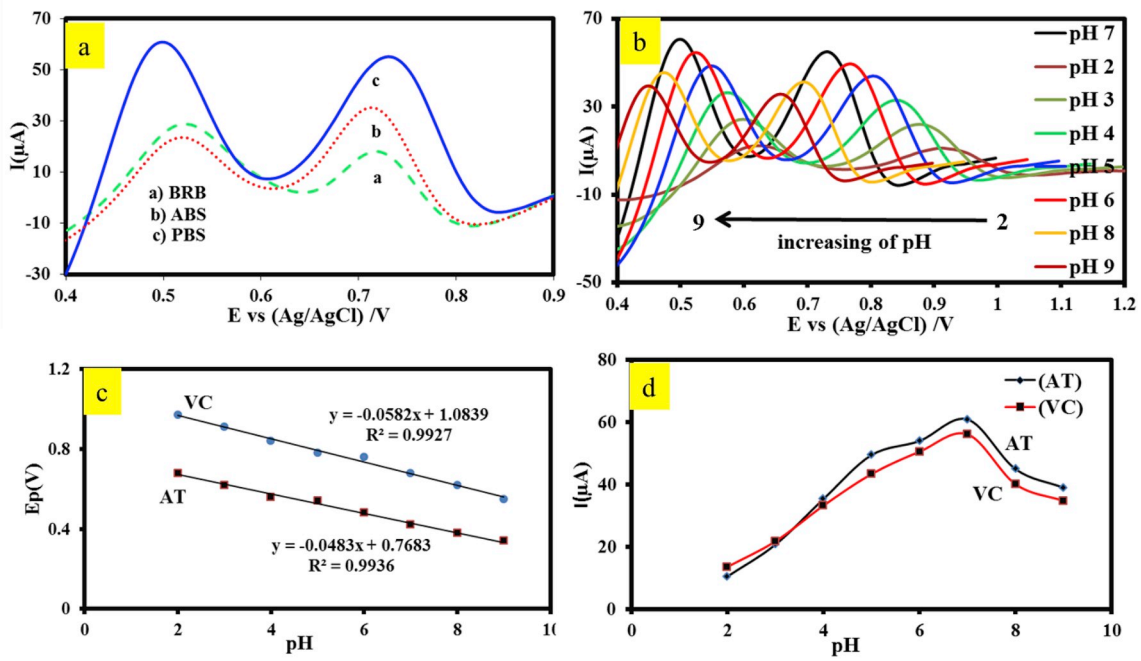

Fig. 4. (a) Effect of supporting electrolyte type on proposed sensor response, (b) DPVs of 53 μM AT and 53 μM VC in 0.1 M PBS at pH 2–9 from right to left, (c) Plots of the oxidation peak potentials for AT and VC as function of solution pH, (d) Plots of the oxidation peak current for AT and VC as function of solution pH.

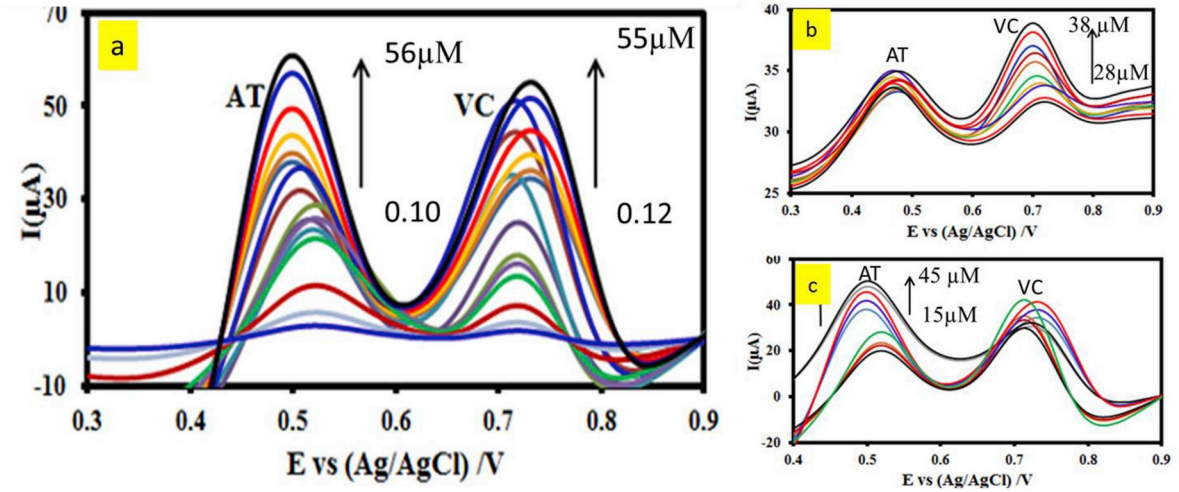

Fig. 5. (a) DPVs of AT and VC at the concentrations of AT from 0.1 μM to 56 μM and of VC from 0.12 μM to 55 μM. (b) DPVs of VC (28–38 μM) in the presence of fixed concentration of AT (28 μM). (c) DPVs of AT (15–45 μM) in the presence of constant concentration of VC (38 μM) at HAP-ZnO-Pd NPs/CPE in 0.1 M PBS (pH 7).

Pd NPs/CPE were evaluated by adding various foreign species into the PBS solution (pH 7) containing 20 μM of AT and 30 μM of VC. Electrochemical responses of HAP-ZnO-Pd NPs/CPE for AT and VC in present various concentration of other species were studied and calculated tolerance limit. The results summarized in Table S3. According to Table S3 maximum of interference was shown by hydroquinone due to similarity of chemical structure and properties. Recovery data of interference study was summarized in Table S4.

3.8. Analytical applications

To demonstrate the applicability of the modified electrode HAP-ZnO-Pd NPs/CPE used for detecting the AT and VC, the sensor was used to the independent determination of VC in fruit juices. The real samples contain fruit juices and 0.1M KCl at pH of 7 and electrochemical measurement of VC was performed via DPV and the results are shown in Table S5. According to Table S4, the recoveries for VC in these samples were obtained to be more than 97%, and maximum of RSD was gotten 4.21%, revealing that the modified electrode was able to accurately determine the content of VC in real samples and bio-samples. For the simultaneous determination of AT and VC in Seagull cream (as lightening Cram cosmetic) sample, various concentrations of the both analyts were spiked to Seagull cream sample and the results are given in Table S6. Accordingly, the practicability of the modified electrode was confirmed. To make a conclusion on the performance and advantages of our work, a literature review is presented in Table 1.

Table 1
Comparing performance of purposed sensor with others for determination of AT and VC.

Electrochemical Technique	Species	Linear range (μM)	Limit of detection (μM)	Ref.
SWV	AT	90- Further	0.18	Shih and Zen (2000)
electrophoresis	AT and VC	180–460 570–1420	3.98	Blasco et al. (2005)
DPV	AT	4–100	2.4	Libánský et al. (2011)
CV	VC	0.5–120	0.063	Pakapongpan et al. (2014)
CV	VC	0.1–106	0.07	Li et al. (2011)
DPV	AT and VC	0.12–56 0.12–55.36	0.08 0.02	This work

4. Conclusions

In summary, a new modified electrochemical sensor (HAP-ZnO-Pd NPs/CPE) was successfully designed to simultaneously determine the AT and VC. In optimal conditions, the fabricated electrode reveal acceptable selectivity and sensitivity and wide linear relationship over 0.12–56 μM with LOD of 85.7 nM for AT and 0.12–55.36 μM with LOD of 19.4 nM for VC. However, the limitation of electrode performance is depending it to mole ratio of AT and VC in mixture while its range of this mole ratio was narrow. This proposed sensor has the potential to be used for the detection of AT and VC in biological and food analyses, horticultural practice and beauty industries.

CRediT authorship contribution statement

Seyed Alireza Shahamirifard: Writing - review & editing. **Mehrorang Ghaedi:** Writing - review & editing.

Appendix A. Supplementary data

Supplementary data to this article can be found online at https://doi.org/10.1016/j.bios.2019.111474.

References

Akiyama, H., Yamasaki, O., Tada, J., Arata, J., 2000. J. Dermatol. Sci. 23 (3), 155–160.
Arabali, V., Ebrahimi, M., Abbasghorbani, M., Gupta, V.K., Farsi, M., Ganjali, M., Karimi, F., 2016. J. Mol. Liq. 213, 312–316.
Arroyo-Ramírez, L., Chen, C., Cargnello, M., Murray, C.B., Fornasiero, P., Gorte, R.J., 2014. J. Mater. Chem. 2 (45), 19509–19514.
Bang, S.H., Han, S.J., Kim, D.H., 2008. J. Cosmet. Dermatol. 7 (3), 189–193.
Bard, A.J., Faulkner, L.R., 2001. Electrochem. Methods 2, 482.
Blasco, A.J., Barrigas, I., González, M.C., Escarpa, A., 2005. Electrophoresis 26 (24), 4664–4673.
Clifford, M.N., 2000. J. Sci. Food Agric. 80 (7), 1126–1137.
Fong, J.F.Y., Chin, S.F., Ng, S.M., 2016. Biosens. Bioelectron. 85, 844–852.
Gallarate, M., Carlotti, M., Trotta, M., Grande, A., Talarico, C., 2004. J. Cosmet. Sci. 55 (2), 139–148.
Hosseini-Sarvari, M., Razmi, Z., 2015. Appl. Surf. Sci. 324, 265–274.
Jahani, S., Beitollahi, H., 2016. Anal. Bioanal. Electrochem. 8 (2), 158–168.
Jeon, J., Kim, B., Lee, S., Kwon, H., Bae, H., Kim, S., Park, J., Shim, J., Abd El-Aty, A., Shin, H., 2015. Int. J. Cosmet. Sci. 37 (6), 567–573.
Jiang, J., Du, X., 2014. Nanoscale 6 (19), 11303–11309.
Kanchana, P., Lavanya, N., Sekar, C., 2014. Mater. Sci. Eng. C 35, 85–91.
Keyworth, N., Millar, M., Holland, K., 1992. Arch. Dis. Child. 67 (7 Spec No), 797–801.
Klimczak, I., Gliszczyńska-Świgło, A., 2015. Food Chem. 175, 100–105.
Kozitskaya, S., Olson, M.E., Fey, P.D., Witte, W., Ohlsen, K., Ziebuhr, W., 2005. J. Clin. Microbiol. 43 (9), 4751–4757.
Li, F., Li, J., Feng, Y., Yang, L., Du, Z., 2011. Sensor. Actuator. B Chem. 157 (1), 110–114.
Libánský, M., í Zima, J., í Barek, J., Dejmková, H., 2011.
Liu, F.-m., Zhang, Y., Yin, W., Hou, C.-j., Huo, D.-q., He, B., Qian, L.-l., Fa, H.-b., 2017. Sensor. Actuator. B Chem. 242, 889–896.
Maeda, K., Fukuda, M., 1991. J. Soc. Cosmet. Chem. 42 (2), 361–368.
Mori, K., Yamaguchi, K., Hara, T., Mizugaki, T., Ebitani, K., Kaneda, K., 2002. J. Am. Chem. Soc. 124 (39), 11572–11573.
Najafi, M., Khalilzadeh, M.A., Karimi-Maleh, H., 2014. Food Chem. 158, 125–131.
O'gara, J.P., Humphreys, H., 2001. J. Med. Microbiol. 50 (7), 582–587.
Pakapongpan, S., Mensing, J.P., Phokharatkul, D., Lomas, T., Tuantranont, A., 2014. Electrochim. Acta 133, 294–301.
Rahmanpour, M.S., Khalilzadeh, M.A., 2016. Anal. Bioanal. Chem. 8, 922–930.
Rochford, J., Chu, D., Hagfeldt, A., Galoppini, E., 2007. J. Am. Chem. Soc. 129 (15), 4655–4665.
Sheng, Z.-H., Zheng, X.-Q., Xu, J.-Y., Bao, W.-J., Wang, F.-B., Xia, X.-H., 2012. Biosens. Bioelectron. 34 (1), 125–131.
Shih, Y., Zen, J.-M., 2000. Anal. Chim. Acta 412 (1–2), 63–68.
Su, B., Chen, Y., Yang, X., Han, J., Jia, H., Jing, P., Wang, Y., 2017. Int. J. Electrochem. Sci. 12 (7), 6417–6427.
Takarroumt, N., Kacimi, M., Bozon-Verduraz, F., Liotta, L.F., Ziyad, M., 2013. J. Mol. Catal. A Chem. 377, 42–50.
Wang, Y.-H., Avonto, C., Avula, B., Wang, M., Rua, D., Khan, I.A., 2015. J. AOAC Int. 98 (1), 5–12.
Yang, Z., Zhang, C., 2011. Biosens. Bioelectron. 29 (1), 167–171.
Yao, S., Yan, X., Zhao, Y., Li, B., Sun, L., 2014. Mater. Lett. 126, 97–100.
Zhao, H., Zhou, H., Zhang, J., Zheng, W., Zheng, Y., 2009. Biosens. Bioelectron. 25 (2), 463–468.